







Magnetic field induced modification of the incommensurate antiferromagnetic structure of Fe-doped MnNiGe alloys

Riya Roy ¹, Sanat Kumar Adhikari ¹, Sambhu Charan Das ^{1,2}, Rosni Roy,¹ Kanai Mondal,¹ Jhuma Sannigrahi ³,
Sabyasachi Pramanick,¹ Kalyanashis De,⁴ Dmitry Khalyavin,⁵ Devashibhai T. Adroja,^{5,6}
Rajib Mondal ¹ and Souvik Chatterjee ^{1,*}

¹UGC-DAE Consortium for Scientific Research, Kolkata Centre, Sector III, LB-8, Salt Lake, Kolkata 700106, India

²Department of Physics, Tamkang University, New Taipei City 251301, Taiwan

³School of Physical Sciences, Indian Institute of Technology Goa, Ponda 403401, Goa, India

⁴School of Science and Technology, The Neotia University, South 24 Parganas 743368, India

⁵ISIS Facility, Rutherford Appleton Laboratory, Chilton, Didcot OX11 0QX, United Kingdom

⁶Highly Correlated Matter Research Group, Physics Department, University of Johannesburg, PO Box 524, Auckland Park 2006, South Africa



(Received 16 May 2024; accepted 22 August 2024; published 9 September 2024)

The evolution of the magnetic structure of Fe-doped MnNiGe alloys of nominal compositions $\text{MnNi}_{0.75}\text{Fe}_{0.25}\text{Ge}$ and $\text{Mn}_{0.85}\text{Fe}_{0.15}\text{NiGe}$ has been probed through neutron powder diffraction (NPD) experiments in the presence of external magnetic fields (H). Application of external H results in a significant decrease in the antiferromagnetic satellite peak's intensities along with a considerable change in the incommensurate propagation vector $\mathbf{k}_{\text{AFM}} = (k_a, 0, 0)$. In addition, a reasonable increase in some of the nuclear reflections has also been noticed, which can clearly be described by the ferromagnetic propagation vector $\mathbf{k}_{\text{FM}} = (0, 0, 0)$. Our analysis confirms the gradual rotation of magnetic moments towards the a axis with increasing H and eventual realization of ferromagnetic arrangement at higher applied H .

DOI: [10.1103/PhysRevB.110.094415](https://doi.org/10.1103/PhysRevB.110.094415)

I. INTRODUCTION

Pure and doped MnNiGe alloys of the magnetic equiatomic family continue to be in the front line of active research field because of their fascinating physical and functional properties, including commensurate and incommensurate (helically and cycloidally modulated) antiferromagnetic (AFM) phases, magnetoresistance, magnetocaloric effect, exchange bias effect, etc. [1–21]. The first-order martensitic phase transition (MPT) plays a decisive role in the observed functionality. The undoped MnNiGe alloy undergoes MPT at 470 K and orders antiferromagnetically with a helical structure around 346 K [2–4, 8, 22–26]. Doping of various foreign elements at different sites of MnNiGe alloy significantly affects both structural and magnetic transition temperatures (T) along with remarkable improvement in their functionality [4, 8, 13–15, 20].

Apart from the change in MPT and magnetofunctionality, the magnetic structure of the MnNiGe alloy is found to be significantly affected by doping of various foreign elements at different sites. Our recent neutron powder diffraction (NPD) data reveals the modification of the helically modulated magnetic structure of pristine MnNiGe alloys with the doping of foreign elements at different sites of the alloy [27, 28]. Perturbation of nonmagnetic transition metal site (i.e., Ni site) with Fe results in an unchanged AFM structure with helical modulation, although a significant change in the propagation vector has been observed [27]. On the other hand, Fe doping at the

Mn site (the only magnetic site) markedly changes the modulation of the AFM phase, and it becomes cycloidal in nature at 1.5 K [27]. Interestingly, with increasing T , a spin reorientation transition has also been noticed, and the modulation becomes helical in nature [27]. The magnetic structure becomes even more fascinating when Al/Ga doping introduces a perturbation at the Ge site [28]. In such cases, in addition to the low- T martensite phase, the high- T austenite phase also becomes magnetic. Helically modulated incommensurate AFM structure and commensurate AFM structure had been concluded for the low- T martensite and high- T austenite phases, respectively [28]. Notably, NPD data confirmed the absence of any ferromagnetism in the doped MnNiGe alloys. However, the incorporation of ferromagnetism in the doped MnNiGe alloys was previously reported, based on the bulk magnetization data [8]. Although these NPD results reveal the magnetic structure of doped MnNiGe alloys in zero field (both in ambient as well as in high-pressure conditions), the modification of the incommensurate AFM structures in the presence of external magnetic field (H) has not yet been explored. Alteration of the magnetic structure in the presence of external H plays a crucial role in the observed magnetofunctionality of these alloys. Therefore, it is pertinent to perform the NPD study in the presence of external H to probe such changes in the magnetic structure. In the present paper, we aim to probe the effect of external H on the magnetic structure of two Fe-doped MnNiGe alloys of nominal compositions $\text{MnNi}_{0.75}\text{Fe}_{0.25}\text{Ge}$ (MNFG) and $\text{Mn}_{0.85}\text{Fe}_{0.15}\text{NiGe}$ (MFNG), each having two different types of modulated (helical and cycloidal) incommensurate AFM structures. Our investigation

*Contact author: souvik@csr.res.in; souvikchat@gmail.com

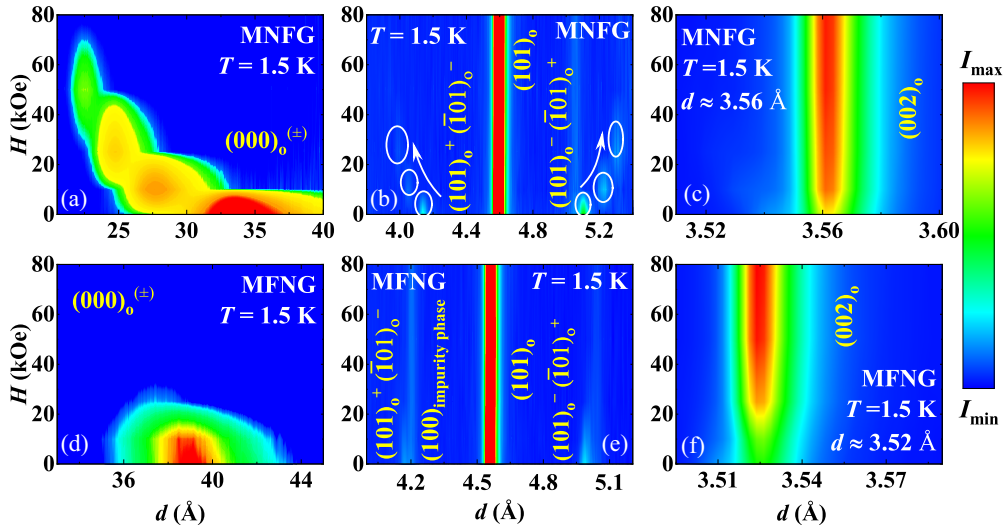


FIG. 1. Contour plots of the magnetic field (H) evolution of some orthorhombic AFM satellite and nuclear reflections are shown in (a)–(c) for MNFG and in (d)–(f) for MFNG alloys. Normalized intensity is indicated by the right-hand side color bar. The subscript “o” in the Miller indices refer to orthorhombic.

reveals a gradual disappearance of AFM satellite reflections and significant increase in some orthorhombic nuclear reflections with increasing H for both the alloys. These observations indicate the appearance ferromagnetic (FM) alignment of the magnetic moments in otherwise AFM alloys.

II. EXPERIMENTAL DETAILS

The presently studied polycrystalline MNFG and MFNG alloys were prepared by melting the required amount of constituent elements, with purity $>99.9\%$, using a Centor-make tri-arc furnace in an inert argon atmosphere. To achieve desired homogeneity, we remelted the alloys several times. Further, the ingots were annealed at 800° for 100 h in an evacuated quartz ampule, followed by rapid quenching in ice water. Time-of-flight cold neutron WISH diffractometer of the ISIS Facility (Rutherford Appleton Laboratory) at the United Kingdom was used to perform NPD studies. Details regarding the data are accessible through the STFC ISIS Facility [29]. A liquid helium cryostat, equipped with an 80 kOe superconducting magnet, from the Oxford Instrument was employed to achieve the desired sample environment. To prevent any type of grain rotation during the high-field measurements, the alloy powders were mixed with cytop (hydrogen free glue) and pressed into pellets. Standard 6 mm vanadium cans were used to mount the pellets inside the cryostat. The isothermal NPD data were collected during warming cycle and analyzed through the Rietveld refinement method using the FULLPROF software package [30]. VESTA software package was used to create and visualize the magnetic structure models [31].

III. EXPERIMENTAL RESULTS

A. Effect of external magnetic field on the magnetic structure

We recorded NPD data at 1.5 K for both MNFG and MFNG alloys in the presence of different applied H to probe the evolution of magnetic structure. Contour plots of some

restricted lattice spacing (d) regions of the NPD patterns are shown in Figs. 1(a)–1(c) and 1(d)–1(f) for MNFG and MFNG alloys, respectively. These restricted plots are for the better visibility of the effect of external H on the major magnetic satellite reflections only. We observed a significant shift in the position of magnetic satellite peaks for the helically modulated incommensurate AFM phase of MNFG alloy with increasing H . The $(101)_o^+$, $(\bar{1}01)_o^-$, and $(000)_o^\pm$ peaks are found to be shifted towards lower d values [see Figs. 1(a) and 1(b)]. However, $(101)_o^-$ and $(\bar{1}01)_o^+$ peaks show a clear shift towards higher d values [see Fig. 1(b)]. In addition to the shift in the peak positions, the intensity of these magnetic satellite reflections decreases drastically with increasing H and eventually vanishes at 80 kOe of applied H . On the other hand, the magnetic satellite reflections of the MFNG alloys, having cycloidally modulated incommensurate AFM structure, behave a bit differently in the presence of external H . Compared to the MNFG alloy, the magnetic peaks [$(101)_o^+$, $(\bar{1}01)_o^-$, $(101)_o^-$, $(\bar{1}01)_o^+$, and $(000)_o^\pm$] are found to show a very small shift with increasing H , while the intensity of such peaks fall very rapidly and eventually vanishes above 25 kOe of applied H for MFNG alloy [see Figs. 1(d) and 1(e)]. Apart from the modifications of the AFM satellite reflections, the application of H also affects some of the orthorhombic nuclear reflections for both the alloys. Intensity variation of one such reflection [$(002)_o$] is depicted in Figs. 1(c) and 1(f). However, the peak positions remain unchanged.

To shed more light on the modified magnetic structure in the presence of applied H , we performed a detailed Rietveld refinement analysis of the NPD patterns, recorded at different H . These representative data for MNFG and MFNG alloys, recorded at 1.5 K in the presence of 10 kOe of applied H , along with refinement patterns for two different d ranges, are plotted in Figs. 2(a)–2(d). In the present case, we have used a similar procedure to that followed for the zero-field case, to refine the magnetic structure of the studied alloys in the presence of external H [27]. As previously reported for the

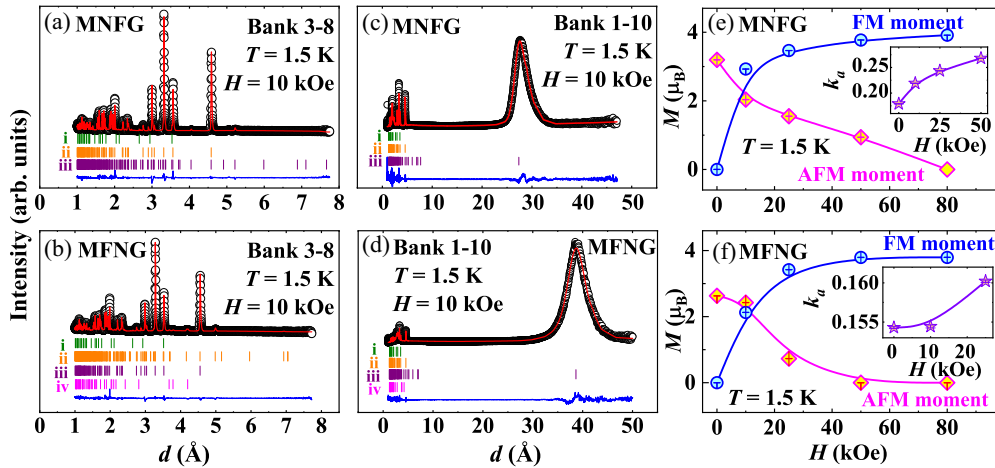


FIG. 2. NPD patterns (black circle) along with calculated (red lines), and difference patterns (blue lines), are depicted in (a), (c) for MNFG and (b), (d) for MFNG alloys, recorded at 1.5 K in the presence of 10 kOe of external H . The data from 3-8 and 1-10 detector banks of WISH are plotted for two different lattice spacing (d) ranges. The vertical bars represent the Bragg's peak position for (i) Ni_2In -type hexagonal phase (olive), (ii) TiNiSi -type orthorhombic nuclear phase (orange), (iii) orthorhombic magnetic phase (purple), and (iv) MgZn_2 -type hexagonal nuclear phase (magenta). The main panels of (e) and (f) represent the variation of AFM and FM moment size as a function of H . Insets in (e) and (f) depict the H dependence of the x component of AFM propagation vector k_{AFM} .

zero-field NPD data, similar contributions of different phases are also found in the presence of 10 kOe of external H . These include (i) the nuclear and magnetic contribution of low- T martensite phase with orthorhombic structure (TiNiSi -type) having $Pnma$ space group, (ii) a small percentage of high- T austenite phase with Ni_2In -type hexagonal structure with $P6_3/mmc$ space group, (iii) the nuclear phase of $\text{MnNi}_{1.3}\text{Ge}_{0.7}$ alloy (an impurity phase) with MgZn_2 -type hexagonal structure with space group $P6_3/mmc$ (only for MFNG alloy). The AFM satellite reflections for both alloys have been indexed successfully by using the incommensurate propagation vector $k_{\text{AFM}} = (k_a, 0, 0)$. Compared to the zero-field data, we observed a significant change in k_a for MNFG alloy, while the value of k_a is found to be very close to the zero-field data for MFNG alloy [27]. In the presence of 10 kOe of applied H , k_a is found to be 0.2190(5) and 0.1544(4) for MNFG and MFNG alloys, respectively. This large change in the x component of propagation vector k_{AFM} results in a significant shifts of the magnetic satellites in the presence of external H . For example, the peak position of the most intense AFM reflection for the MNFG alloy is around $d \sim 27.37$ Å for $H = 10$ kOe and $d \sim 33.49$ Å for $H = 0$ kOe. Notably, the nature of shift in these magnetic peaks is completely opposite to that observed in the presence of external pressure [27]. Pressure-induced decrease in the lattice parameters, which remain almost unchanged in the presence of external H (magnetic unit cell only experiences a change owing to the rotation of Mn moments), plays the crucial role behind such observation.

Apart from the effect on the incommensurate reflections, the application of H also results in an increase in some of the orthorhombic reflections [see Figs. 1(c) and 1(f) for one such representative reflection]. This increase in the intensity of the nuclear reflections indicates the appearance of FM interaction in the alloys on the application of external H . To incorporate such FM contribution, we also included FM propagation vector $k_{\text{FM}} = (0, 0, 0)$ during the refinement. For proper refinement of the experimental data, we tried to

incorporate the FM interactions in all three directions; however, the best fitting (along with acceptable refinement parameters, like moment value, etc.) can be obtained after introducing the FM interaction only along the a axis (for both the alloys). The appearance of FM ordering along the a axis directly affects the overall modulation of the incommensurate AFM structure in the studied alloys. In the zero-field condition: (i) for the helically modulated MNFG alloy, the moment rotation was reported to be in the bc plane, which propagates along the a axis; (ii) for the cycloidally modulated MFNG alloy, spins were found to be rotating in the ab plane and propagating along the a axis [27]. The presence of an FM component along the a axis results in a tilting of the spins rotating in the bc plane towards a axis, making the overall modulation conical for MNFG alloy. This magnetic structure is shown in Fig. 3(a). On the other hand, the modulation of the MFNG alloy remains cycloidal even after the incorporation of FM ordering; however, the moment size of Mn atoms become unequal along the direction of propagation [see Fig. 3(d)]. All relevant refinement parameters are listed in Table 1 within the Supplemental Material [32].

We further analyzed the NPD data recorded in the presence of higher applied H (25 kOe, 50 kOe, and 80 kOe). We observed a monotonic increase in the x component of incommensurate propagation vector k_{AFM} . The variation of k_a as a function of H is plotted as insets in Figs. 2(e) and 2(f) for MNFG and MFNG alloys, respectively. About 50% increase in k_a has been observed for the MNFG alloy for 50 kOe of applied H . On the other hand, the increase in MFNG alloy is only about 3% for 25 kOe of applied H . This change in k_a values is consistent with the shift in the magnetic satellite reflections. Apart from the change in the x component of the incommensurate AFM propagation vector, a significant change in the moment values of both AFM and FM interactions has been noticed. The variation of AFM and FM moment sizes are plotted as a function of H in the main panels of Figs. 2(e) and 2(f). A gradual change in the AFM and FM

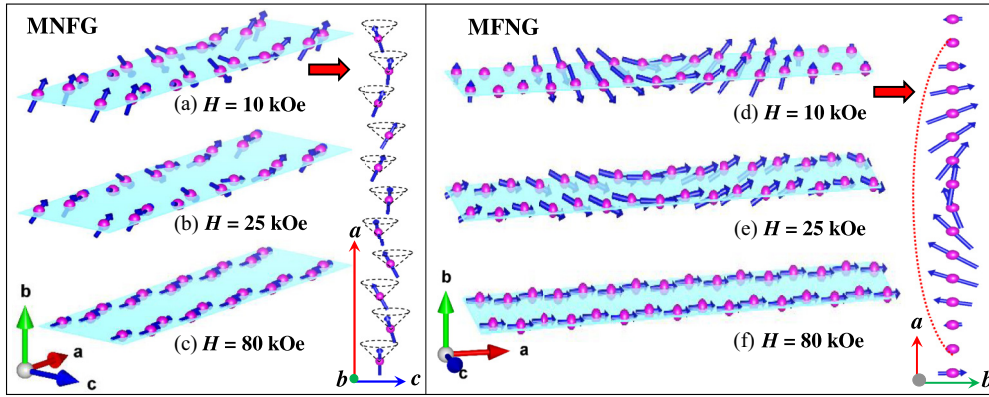


FIG. 3. Panels (a)–(c) and (d)–(f) illustrate the evolution of helically and cyclodially modulated incommensurate AFM structures at different applied H for MNFG and MFNG alloys, respectively. The schematic representations of the conical and modified cyclodial structures in the presence of 10 kOe of external fields are represented vertically.

moment size results in a systematic change in the overall magnetic structure, and, finally, both the alloys attain FM ordering along the a axis. The evolution of the magnetic structures are plotted in Figs. 3(a)–(c) and 3(d)–(f) for MNFG and MFNG alloys, respectively. In the presence of a significantly high value of H , both the alloys become completely FM with all the Mn moments aligning along the a axis. Perturbation in the magnetic site for MFNG alloy is mainly responsible for the observation of significantly low values of the critical values of applied H for achieving the FM arrangement compared to the MNFG alloy. The FM saturation moments for MNFG and MFNG alloys, in the presence of 80 kOe of external H , are found to be $3.91(4) \mu_B$ and $3.79(4) \mu_B$, respectively.

B. Temperature evolution of magnetic structure in the presence of external magnetic field

To probe the effect of external H on the T evolution of the magnetic structure, we recorded NPD data in the presence of 10 and 50 kOe of external H at different constant T . Figures 4(a) and 4(b) depict the contour plots of some restricted regions of the recorded NPD patterns (recorded at $H = 10$ kOe) for the representative MFNG alloy. Some of the incommensurate AFM reflections are focused in these contour plots for a better understanding of the T evolution of the magnetic phases in the presence of external H . We observed a monotonic change in the AFM satellite reflection positions with increasing alloy T [increase in d value for $(101)_0^+$, $(\bar{1}01)_0^-$, and $(000)_0^\pm$ satellite reflections; and decrease in d value for $(101)_0^-$ and $(\bar{1}01)_0^+$ satellite reflections]. This is unlike the zero-field data, where the AFM satellite peak positions remain unaltered with increasing T [27]. These shifts in the peak positions result in a decrease in the x component of the incommensurate propagation vector k_{AFM} . T variation of k_a for MNFG and MFNG alloys are plotted in the insets in Figs. 4(e) and 4(f), respectively. About 13.5% and 2% decrease in the k_a value has been observed for MNFG and MFNG alloys, respectively. Apart from the shift in the AFM satellite peak positions, a monotonic decrease in the peak intensities has been observed with increasing sample T for both alloys. The variation of the integrated intensity of $(000)_0^\pm$ as a function of alloy T are depicted in Figs. 4(c)

and 4(d), respectively. This behavior is markedly different from the nonmonotonic intensity variation observed for the MFNG alloy in zero-field conditions [27]. The absence of any nonmonotonicity in the MFNG confirms the nonexistence of any T -induced spin-reorientation transition (from cyclodial to helical) in the presence of 10 kOe of external H . T -driven spin-reorientation transition from cyclodial to helically modulated incommensurate AFM transition is one of the key properties of MFNG alloys in zero-field conditions [27]. Application of H results in an unaltered modulation of the incommensurate AFM phase for both the alloys. We have also calculated and plotted the martensite and austenite phase fractions as a function of T in Figs. 4(e) and 4(f). MPT is found to be almost unchanged with increasing H , which is also consistent with the dc magnetization data reported previously [33]. Interestingly, application of H triggered incomplete MPT, which results in an increase in the austenite phase fraction below the MPT region for both the alloys. For 10 kOe of applied H , we observed around 5.5 and 4.5% of high- T hexagonal phase for MNFG and MFNG alloys, respectively. Notably, in the zero-field conditions, 0.48 and 1.04% of high- T hexagonal phase was found to be present at 1.5 K [27].

IV. DISCUSSION AND CONCLUSIONS

High- H NPD data reveal several fascinating characteristics in Fe-doped MnNiGe alloys. The gradual disappearance of incommensurate AFM phases and the appearance of FM ordering along the a axis is the most important observation of the present paper. The zero-field incommensurate AFM configurations observed in the analyzed alloys can effectively be elucidated using a theoretical model [25,26,34,35]. This model incorporates anisotropic competing exchange interactions, where spins are bound by a nearest-neighbor FM interaction within a plane perpendicular to the modulation axis of the helical/cyclodial magnetic structure. Additionally, spins are interconnected via both nearest-neighbor FM (J_1) and next-nearest-neighbor AFM interactions (J_2) along the modulation axis, thereby giving rise to the formation of the helical/cyclodial phase. In the presence of external H , the appearance of Zeeman term MH (M is the ferromagnetic

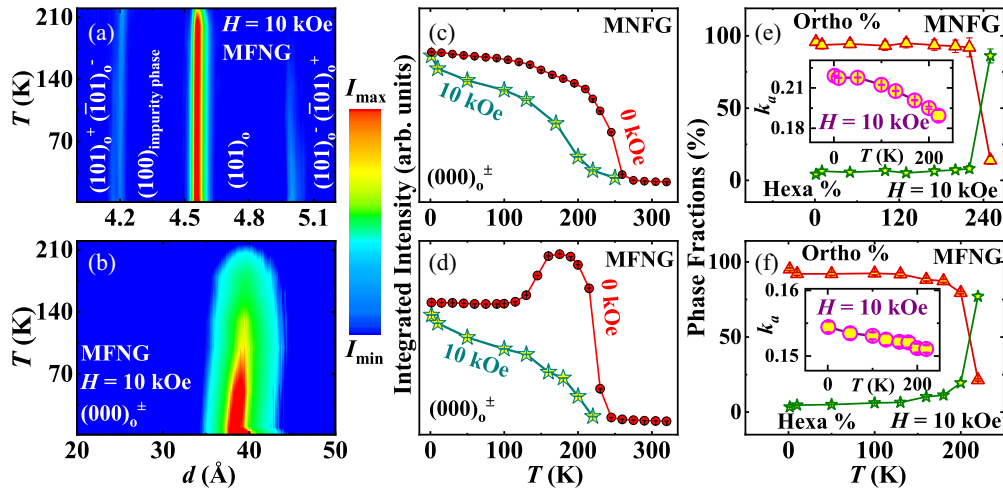


FIG. 4. Panels (a) and (b) depict the contour plot of the T evolution of some magnetic satellite reflections for the representative MFNG alloy. The NPD data were recorded in the presence of 10 kOe of applied H . (c) and (d) show the T variation of the integrated intensity of $(000)^\pm$ magnetic satellite reflection for MNFG and MFNG alloys, respectively at $H = 0$ [27] and 10 kOe. T variation of the x component of the incommensurate propagation vector are plotted as the insets in (e) and (f). T variation of orthorhombic and hexagonal phase fractions at $H = 10$ kOe of external H are shown in the main panels of (e) and (f) for MNFG and MFNG alloys, respectively. The subscript “o” stands for orthorhombic in the Miller indices.

moment) alters the nearest-neighbor FM interaction (J_1), which results in a significant change in the x component of the incommensurate propagation vector k_{AFM} . This Zeeman term also perturbs the helical/cycloidal modulation observed in the zero-field case (helical modulation becomes conical in nature, while cycloidal modulation remains cycloidal, with unequal Mn moment values) and eventually in the presence of high enough external H , a complete FM arrangement has been observed for both the alloys. Similar increase in J_1 has also been observed on the application of external pressure [27]. However, the absence of any Zeeman term prevents the modification of the modulation of the incommensurate AFM structure of these alloys. Apart from that, the rate of development of the FM ordering depends strongly on the perturbation site. Fe doping at the magnetically ordered Mn site results in a faster approach to complete FM arrangement in MFNG alloy in the presence of 25 kOe of external H .

The T -dependent NPD measurements in the presence of external H indicate the disappearance of the spin-reorientation transition. The zero-field NPD measurements on MFNG alloy, reported by our group, clearly reveal the T -induced spin-reorientation transition from cycloidally modulated incommensurate AFM to helically modulated incommensurate AFM structure in the low- T martensitic phase [27]. In the presence of an external H , the cycloidally modulated AFM structure remains unchanged with increasing alloy T throughout the entire magnetically ordered martensite phase. The absence of such spin-reorientation transition results in a monotonic change in the T variation of integrated intensities of the AFM satellite reflections. This observation indicates

that the application of H prefers cycloidal modulation in the MFNG alloy. Notably, the application of external pressure is found to prefer helical modulation over cycloidal modulation in MFNG alloy [27]. However, the modulation of the MNFG alloy remains conical in the presence of external H . The T evolution of the NPD data also reveals the appearance of incomplete MPT. These observations indicate that the external H favors the high- T austenite phase. Interestingly, similar behavior has also been observed in the presence of external pressure [27].

In conclusion, we successfully probed the evolution of the magnetic structure in the presence of external H of two Fe-doped MnNiGe alloys of nominal compositions $\text{MnNi}_{0.75}\text{Fe}_{0.25}\text{Ge}$ and $\text{Mn}_{0.85}\text{Fe}_{0.15}\text{NiGe}$. The helically/cycloidally modulated incommensurate AFM structures of the studied alloys achieve FM ordering along the a direction in the presence of high enough external H . The disappearance of spin-reorientation transition in the presence of external H in MFNG alloy is another important observation of the present paper.

ACKNOWLEDGMENTS

S.C. and Riya Roy would like to thank the Science and Engineering Research Board (SERB), DST-India, for financial support (Project No. CRG/2020/000670). S.C. would like to thank ISIS facility, UK for the access to the experimental facility and financial support to carry out the experiments. J.S. would like to thank SERB, DST-India, for the Ramanujan Fellowship (Grant No. RJF/2019/000046).

[1] K. Koyama, M. Sakai, T. Kanomata, and K. Watanabe, Field-induced martensitic transformation in new ferromagnetic shape memory compound $\text{Mn}_{1.07}\text{Co}_{0.92}\text{Ge}$, *Jpn. J. Appl. Phys.* **43**, 8036 (2004).

[2] C. L. Zhang, D. H. Wang, Q. Q. Cao, Z. D. Han, H. C. Xuan, and Y. W. Du, Magnetostructural phase transition and magnetocaloric effect in off-stoichiometric $\text{Mn}_{1.9-x}\text{Ni}_x\text{Ge}$ alloys, *Appl. Phys. Lett.* **93**, 122505 (2008).

- [3] C. Zhang, D. Wang, Q. Cao, S. Ma, H. Xuan, and Y. Du, The magnetostructural transformation and magnetocaloric effect in Co-doped MnNiGe_{1.05} alloys, *J. Phys. D: Appl. Phys.* **43**, 205003 (2010).
- [4] P. Dutta, S. Pramanick, D. Venkateshwarlu, V. Ganesan, S. Majumdar, D. Das, and S. Chatterjee, Spin-glass-like ground state and observation of exchange bias in Mn_{0.8}Fe_{0.2}NiGe alloy, *Europhys. Lett.* **108**, 17012 (2014).
- [5] T. Samanta, I. Dubenko, A. Quetz, S. Temple, S. Stadler, and N. Ali, Magnetostructural phase transitions and magnetocaloric effects in MnNiGe_{1-x}Al_x, *Appl. Phys. Lett.* **100**, 052404 (2012).
- [6] N. T. Trung, L. Zhang, L. Caron, K. H. J. Buschow, and E. Brück, Giant magnetocaloric effects by tailoring the phase transitions, *Appl. Phys. Lett.* **96**, 172504 (2010).
- [7] P. Dutta, S. Pramanick, S. Majumdar, D. Das, and S. Chatterjee, Multifunctional behavior of Fe-doped MnNiGe magnetic equiatomic compound, *J. Magn. Magn. Mater.* **395**, 312 (2015).
- [8] E. Liu, W. Wang, L. Feng, W. Zhu, G. Li, J. Chen, H. Zhang, G. Wu, C. Jiang, H. Xu, and F. de Boer, Stable magnetostructural coupling with tunable magnetoresponsive effects in hexagonal ferromagnets, *Nat. Commun.* **3**, 873 (2012).
- [9] L. Caron, N. T. Trung, and E. Brück, Pressure-tuned magnetocaloric effect in Mn_{0.93}Cr_{0.07}CoGe, *Phys. Rev. B* **84**, 020414(R) (2011).
- [10] I. Dincer, E. Yüziak, G. Durak, Y. Elerman, A. M. T. Bell, and H. Ehrenberg, Exploring the details of the martensitic phase transition and magnetocaloric effect of CoMnGe_{0.95}Ga_{0.05} by synchrotron and magnetic measurements, *J. Alloys Compd.* **540**, 236 (2012).
- [11] N. T. Trung, V. Biharie, L. Zhang, L. Caron, K. H. J. Buschow, and E. Brück, From single- to double-first-order magnetic phase transition in magnetocaloric Mn_{1-x}Cr_xCoGe compounds, *Appl. Phys. Lett.* **96**, 162507 (2010).
- [12] J. Wang, D. Wang, C. Chen, O. Nashima, T. Kanomata, H. Mizuseki, and Y. Kawazoe, Vacancy induced structural and magnetic transition in MnCo_{1-x}Ge, *Appl. Phys. Lett.* **89**, 262504 (2006).
- [13] P. Dutta, S. Pramanick, V. Singh, D. T. Major, D. Das, and S. Chatterjee, Anomalous magnetotransport behavior in Fe-doped MnNiGe alloys, *Phys. Rev. B* **93**, 134408 (2016).
- [14] P. Dutta, S. Pramanick, D. Das, and S. Chatterjee, Hydrostatic pressure tuned magneto-structural transition and occurrence of pressure induced exchange bias effect in Mn_{0.85}Fe_{0.15}NiGe alloy, *J. Phys. D: Appl. Phys.* **49**, 385001 (2016).
- [15] K. Mandal, P. Dutta, P. Dasgupta, S. Pramanick, and S. Chatterjee, Enhancement of magnetocaloric effect by external hydrostatic pressure in MnNi_{0.75}Fe_{0.25}Ge alloy, *J. Phys. D: Appl. Phys.* **51**, 225004 (2018).
- [16] K. Mandal, S. C. Das, P. Dutta, S. Pramanick, P. Dasgupta, and S. Chatterjee, Effect of hydrostatic pressure on the magnetic and magnetocaloric properties of Fe-doped MnCoGe alloys, *J. Appl. Phys.* **124**, 215904 (2018).
- [17] K. Mandal, S. C. Das, P. Dutta, S. Pramanick, and S. Chatterjee, Effect of non-magnetic Ag-doping on magnetic and magneto-functional properties of MnNiGe alloy, *J. Alloys Compd.* **822**, 153454 (2020).
- [18] S. C. Das, K. Mandal, P. Dutta, S. Pramanick, and S. Chatterjee, The effect of pressure and temperature on the magnetic and magnetocaloric properties of an MnNi_{0.9}Ge_{1.1} alloy, *J. Phys. D: Appl. Phys.* **51**, 065002 (2018).
- [19] S. C. Das, K. Mandal, P. Dutta, S. Pramanick, and S. Chatterjee, Observation of room temperature magnetocaloric effect in Mn_{0.9}Ni_{1.1}Ge alloy, *J. Magn. Magn. Mater.* **465**, 44 (2018).
- [20] R. Roy, S. K. Adhikari, S. C. Das, R. Roy, S. Pramanick, K. De, O. Ivashko, A.-C. Dippel, M. von Zimmermann, S. Bandyopadhyay, R. Mondal, and S. Chatterjee, Impact of incomplete martensitic phase transition on the magnetic behavior of Co-doped MnNiGe_{1.05} alloys, *Phys. Rev. B* **109**, 144420 (2024).
- [21] J.-H. Chen, T. P. Chhetri, A. T. Grant, X. Bai, Q. Zhang, C.-K. Chang, D. P. Young, I. Dubenko, S. Talapatra, N. Ali, and S. Stadler, Controlling phase transitions in MnNiGe using thermal quenching and hydrostatic pressure, *J. Phys. D: Appl. Phys.* **57**, 205003 (2024).
- [22] W. Bazela, A. Szytuła, J. Todorović, Z. Tomkowicz, and A. Zięba, Crystal and magnetic structure of NiMnGe, *Phys. Stat. Sol. (a)* **38**, 721 (1976).
- [23] W. Bażela, A. Szytuła, J. Todorović, and A. Zięba, Crystal and magnetic structure of the NiMnGe_{1-n}Si_n system, *Phys. Stat. Sol. (a)* **64**, 367 (1981).
- [24] W. Bażela and A. Szytuła, Crystal and magnetic structure of the NiMn_{1-n}Ti_nGe system, *Phys. Stat. Sol. (a)* **66**, 45 (1981).
- [25] B. Penc, A. Hoser, S. Baran, R. Duraj, M. Marzec, T. J. Gołąb, A. Szytuła, V. Dyakonov, N. Nedelko, A. Sivachenko *et al.*, Influence of Ti atoms on the magnetic order in quaternary NiMnGe:Ti compounds, *Phase Transition* **91**, 1107 (2018).
- [26] B. Penc, A. Hoser, S. Baran, and A. Szytuła, Helicoidal ordering in NiMn_{1-x}Cr_xGe for $x = 0, 0.04, 0.11$ and 0.18 , *Phase Transitions* **91**, 118 (2018).
- [27] R. Roy, S. K. Adhikari, J. Sannigrahi, K. Mandal, S. C. Das, P. Dutta, S. Pramanick, D. Khalyavin, D. T. Adroja, and S. Chatterjee, Doping site induced alteration of incommensurate antiferromagnetic ordering in Fe-doped MnNiGe alloys, *Phys. Rev. B* **104**, 214405 (2021).
- [28] S. C. Das, J. Sannigrahi, P. Dutta, S. Pramanick, D. Khalyavin, D. T. Adroja, and S. Chatterjee, Martensitic transition assisted modification of the antiferromagnetic ordering in Ge-site doped MnNiGe alloys, *Phys. Rev. B* **103**, 094422 (2021).
- [29] S. Chatterjee, J. Sannigrahi, D. Khalyavin, R. Roy, S. K. Adhikari, and D. T. Adroja, Effect of magnetic field on the magnetic structure of Fe-doped MnNiGe alloys, doi: 10.5286/ISIS.E.RB2220764 (2022)
- [30] J. Rodríguez-Carvajal, Recent advances in magnetic structure determination by neutron powder diffraction, *Physica B: Condens. Matter* **192**, 55 (1993).
- [31] K. Momma and F. Izumi, VESTA 3 for three-dimensional visualization of crystal, volumetric and morphology data, *J. Appl. Cryst.* **44**, 1272 (2011).
- [32] See Supplemental Material at <http://link.aps.org/supplemental/10.1103/PhysRevB.110.094415> for the details of various structural refinement parameters obtained from the Rietveld analysis of the neutron powder diffraction patterns in a tabulated form.

- [33] P. Dutta, D. Das, S. Chatterjee, S. Pramanick, and S. Majumdar, Hydrostatic pressure effect on the magnetocaloric behavior of Ga-doped MnNiGe magnetic equiatomic alloy, *J. Phys. D: Appl. Phys.* **49**, 125001 (2016).
- [34] U. Enz, Magnetization process of a helical spin configuration, *J. Appl. Phys.* **32**, S22 (1961).
- [35] A. Herpin, P. Meriel, and J. Villain, Helical antiferromagnetism, *J. Phys. Radium* **21**, 67 (1960).